RSC Advances

PAPER

View Article Online
View Journal | View Issue

Cite this: *RSC Adv.*, 2017, **7**, 30262

Upconversion fluorescence imaging of HeLa cells using ROS generating SiO_2-coated lanthanide-doped $NaYF_4$ nanoconstructs

Przemysław Kowalik,*[a] Danek Elbaum,[a] Jakub Mikulski,[a] Krzysztof Fronc,[a] Izabela Kamińska,[a] Paulo C. Morais,[bc] Paulo Eduardo de Souza,[c] Rodrigo Barbosa Nunes,[c] Fabiane Hiratsuka Veiga-Souza,[m] Grzegorz Gruzeł,[d] Roman Minikayev,[a] Tomasz Wojciechowski,[a] Ewa Mosiniewicz-Szablewska,[a] Maciej Szewczyk,[ij] Mirosława Pawlyta,[l] Andrzej Sienkiewicz,[fg] Mariusz Łapiński,[e] Karolina Zajdel,[h] Piotr Stępień,[ijk] Jacek Szczepkowski,[a] Włodzimierz Jastrzębski,[a] Małgorzata Frontczak-Baniewicz,[h] Wojciech Paszkowicz[a] and Bożena Sikora[a]

Received 17th October 2016
Accepted 19th May 2017

DOI: 10.1039/c6ra25383k

rsc.li/rsc-advances

Inorganic nanomaterials able to generate reactive oxygen species (ROS) are promising components for modern medical applications. Activated by near-infrared light, up-converting β-$NaYF_4$ doped with Er^{3+}–Yb^{3+} and Tm^{3+}–Yb^{3+} pair ions nanoparticles (UCNPs), have a wide range of applications in biological imaging as compared to traditional reagents excited by ultra-violet or visible light. We analysed the green-red and the blue-red luminescence to explain the mechanism of the upconversion depended on the surface condition. The influence of SiO_2 coating on the cytotoxicity of the as-produced UCNPs towards HeLa cancer cells was reported. We demonstrated a possibility of a direct UCNPs application to photodynamic therapy, without need to attach additional molecules to their surface. The presence of Tm^{3+}–Yb^{3+} pair ions, thus ROS generation capability, renders the SiO_2 shell coated nanoparticles to become potentially useful theranostic agent.

1 Introduction

Presently, cancer is one of the most prevalent diseases. In Europe, this pathology is responsible for 20% of deaths, with more than 3 million new cases and 1.7 million deaths every year. Actually, after cardiovascular diseases, cancer is the most important cause of deaths and morbidity in Europe (WHO). Fluorescent techniques are known as ultra-sensitive diagnostic tools to identify some pathogenic cells at the molecular level. Optical imaging is extremely useful in biomedical research for early detection of pathogenic cells as well as for therapy. Many types of luminophores are currently applied in bioimaging (*e.g.* quantum dots, fluorescent proteins, organic dyes, dye doped silica nanoparticles, metallic nanoparticles). However, application of organic probes for luminescence imaging of living organism has some limitations. For instance, the excitation of the traditional bio-labels usually requires UV or VIS light, leading to: (I) low signal-to-noise ratio due to high biological autofluorescence, (II) small light penetration depth, and (III) possible cell photodamages.[1,2]

Therefore, it is desirable to use fluorescent biolabels that can be excited by near infrared (NIR) light. In particular, NIR light is safe to the human body and can penetrate into tissues up to several centimetres.[3,4] Upconversion nanoparticles (UCNPs), which can convert photons of lower energy (*e.g.* NIR light) to higher energy (*e.g.* visible light) *via* a two-photon or multiphoton upconverssion mechanisms,[5] represent a new class of fluorescent biolabels. UCNPs have a relatively high quantum yield, as compared to a two-photon excitation of organic dyes, or quantum dots used in two-photon microscopy, narrow emission

[a]*Institute of Physics, Polish Academy of Sciences, Aleja Lotnikow 32/46, PL-02668 Warsaw, Poland. E-mail: pkowalik@ifpan.edu.pl*
[b]*College of Chemistry and Chemical Engineering, Anhui University, Hefei 230601, China*
[c]*Instituto de Fisica, Universidade de Brasilia, Brasilia, DF 70919-970, Brazil*
[d]*Institute of Nuclear Physics, PAS, ul. Radzikowskiego 152, Krakow 31-342, Poland*
[e]*Institute of Optoelectronics, Military University of Technology, ul. Gen. S. Kaliskiego 2, Warsaw 00-908, Poland*
[f]*Laboratory of Physics of Complex Matter, EPFL, Station 3, Lausanne CH-1015, Switzerland*
[g]*ADSresonaces Sarl, Route de Geneve 60B, Préverenges CH-1028, Switzerland*
[h]*Mossakowski Medical Research Centre, PAS, ul. Pawińskiego 5, Warsaw 02-106, Poland*
[i]*Institute of Genetics and Biotechnology, Faculty of Biology, UW, ul. Pawińskiego 5a, Warsaw 02-106, Poland*
[j]*Institute of Biochemistry and Biophysics, PAS, ul. Pawińskiego 5a, Warsaw 02-106, Poland*
[k]*Centre of New Technologies, UW, ul. S. Banacha 2c, Warsaw 02-097, Poland*
[l]*Institute of Engineering Materials and Biomaterials, Silesian University of Technology, ul. Konarskiego 18A, Gliwice 44-100, Poland*
[m]*Faculty of Ceilandia, Universidade de Brasilia, Brasilia, DF 70919-970, Brazil*

peak, large anti-Stokes shift, good chemical stability, and relatively low toxicity.[6,7] Since UCNPs are NIR light active, the signal-to-noise ratio and sensitivity of the optical detection can be improved due to the absence of autofluorescence.[8–10] Therefore, UCNPs are promising alternatives to traditional fluorescent biolabels for cell imaging and possess prominent potential in biological and clinical applications such as photodynamic therapy (PDT). In this therapy as a lethal factor are using reactive oxygen species (ROS).[11] In traditional case of PDT, photosensitizer is activate by visible light to generate ROS, as described above this kind of light has limitation at tissues penetration. Materials with upconverting properties could be used to activation of photosensitizer directly in the environment of tumor. UCNPs excited by NIR light transfer absorbed energy to photosensitizer molecules and cause generation of ROS.[12,13]

The most efficient host material for the 980 nm upconversion is the hexagonal-phase (β-phase) $NaYF_4$. The β-$NaYF_4$ host is frequently doped with rare-earth (RE) ions, as for instance Yb^{3+}–Er^{3+} or Yb^{3+}–Tm^{3+} ion pair.[14–17] Monodisperse UCNPs are usually synthesized in organic solvents at high-temperatures. However, the most commonly used hydrophobic capping agent, namely oleic acid, limits their biological applications.[17–22]

The coating of the nanoparticles (NPs) by thin silica (SiO_2) layer or metal oxides makes them dispersible in water. The use of SiO_2 for external coating of lanthanide-doped UCNPs is an attractive alternative because the surface chemistry of silica spheres is well documented and silica is known to be relatively harmless while using in biological systems.[23–25] Moreover, the thickness and the surface properties of SiO_2 shell can be easily adjusted to favour secretion of SiO_2-coated UCNPs through the kidneys.[26]

Both types of materials, surface unmodified UCNPs and core–shell with solid oxide, have a potential to attach some molecules.[27] This fact enhances their application in selected cancer therapy called photodynamic therapy. In this case UCNPs must be connect with photosensitizer molecules.[28,29] Presented nanoparticles, doped with thulium ions, are an alternative system, avoiding unstable (photobleaching) molecules of photosensitizers.[30] Wide emission spectrum, dependent on the ions pair (Yb^{3+}–Tm^{3+}), allows to apply the upconverting system for generation of reactive oxygen species without any additional reagents like photosensitizer molecules present in the traditional photodynamic therapy.[31] High energy emitted UV light is capable to decompose water molecules to toxic radicals.

Herein, we report on a general method of silica-coating β-$NaYF_4$:20%Yb^{3+},2%Er^{3+} and β-$NaYF_4$:20%Yb^{3+},0.2%Tm^{3+} NPs. The $NaYF_4$ host matrix has a very low phonon energy and therefore minimizes the quenching of the lanthanide ions excited-state, which results in a high quantum yield for upconversion luminescence (UCL).[32–39] Depending on the RE doping, under NIR excitation UCL emission of different colours is obtained, thus making the obtained UCNPs interesting for multicolour bioimaging, basic material in modern photodynamic therapy.

In brief, we report on the synthesis of functionalized SiO_2-coated UCNPs with sizes smaller than 20 nm, which form stable aqueous suspensions and therefore can be applied for biological optical imaging. The SiO_2-coating improves the overall biocompatibility of the UCNPs and makes them suitable for functionalization with biologically-active molecules.

2 Methods

2.1. Materials

Trifluoroacetic acid (99%, Sigma-Aldrich), sodium trifluoroacetate (>99%, Sigma-Aldrich), yttrium(III) oxide (99.99%, Sigma-Aldrich), ytterbium(III) oxide (99.9%, Sigma-Aldrich), erbium(III) oxide (99.9%, Sigma-Aldrich), thulium(III) oxide (99.9%, Sigma-Aldrich), 1-octadecene (>95%, Sigma-Aldrich), oleic acid (99%, Chempur), cyclohexane (99%, Chempur), ethanol (99.8%, Chempur), polyoxyethylene(5)nonylphenylether IGEPAL CO-520 (Sigma-Aldrich), ammonium hydroxide solution (30%, Sigma-Aldrich) and tetraethyl orthosilicate TEOS (98%, Sigma-Aldrich) were used without further purification.

2.2. Synthesis of β-$NaYF_4$:20%Yb^{3+},2%Er^{3+} and β-$NaYF_4$:20%Yb^{3+},0.2%Tm^{3+} nanoparticles

The upconverting NPs were synthesized by homogeneous solution coprecipitation method. The nanoparticles were prepared from precursors (trifluoroacetate salts of yttrium, ytterbium, and erbium or thulium). The trifluoroacetate salts were chemically prepared according to method reported previously.[40]

The main synthesis was carried out at non-oxide waterless reaction environment using solution of oleic acid and octadecene, at 330 °C for 30 minutes.[41]

2.3. Synthesis of β-$NaYF_4$:20%Yb^{3+},2%Er^{3+}@SiO_2 nanoparticles

The β-$NaYF_4$:20%Yb^{3+},2%Er^{3+} NPs were surface coated with silica to improve their functionality. Solution of NPs suspended in cyclohexane was mixed with IGEPAL CO-520 and the mixture was sonicated for 10 min. Next ammonia was added dropwise and stirred for 30 min. Then, TEOS was added and the solution was stirred for 24 h at room temperature. The NPS was cleaned by mixture of ethanol/water solution (1 : 1) five times after the reaction.[42]

2.4. Characterization of $NaYF_4$:20%Yb^{3+},2%Er^{3+}, $NaYF_4$:20%Yb^{3+},0.2%Tm^{3+}, and $NaYF_4$:20%Yb^{3+},2%Er^{3+}@SiO_2 nanoparticles

The size distribution and morphology of both β-$NaYF_4$:20%Yb^{3+},2%Er^{3+} and β-$NaYF_4$:20%Yb^{3+},0.2%Tm^{3+} NPs were assessed by scanning electron microscopy (SEM) using a Zeiss Auriga Neon 40 microscope at an acceleration voltage of 5 kV. For SEM imaging samples were prepared by dropping the NPs' solution onto the surface of a 0.5 × 0.5 cm^2 silicon wafer. The presence of the SiO_2 shell was confirmed using high-resolution transmission electron microscopy (HRTEM). Elemental analysis of the NPs was performed using the energy-dispersive spectroscopy (EDX) accessory connected to the TEM system (FEI Tecnai Osiris operating at 80 kV acceleration voltage).

The crystal structure of the NPs was determined using TEM and X-ray diffraction (XRD). XRD measurements were conducted in a Philips X'Pert Pro Alpha1 MPD (Panalytical) diffractometer in the 2θ range of 10–150° (15 h pattern scanning at 1.5406 nm wavelength).

The upconversion luminescence of the NPs was measured in an optical system comprising a 980 nm continuous wave (CW) laser (Lumics model LU0980D300-DNA014) as the optical excitation source and a Jobin Yvon-SPEX 270 M monochromator equipped with a CCD camera. Luminescence spectra were measured in the 500 to 700 nm range. A shortpass filter cut-off 750 nm (ThorLabs FESH0750) was employed while recording the luminescence data.

2.5. Incubation of HeLa cells with β-$NaYF_4$:20%Yb^{3+},2%Er^{3+} and β-$NaYF_4$:20%Yb^{3+},2%Er^{3+}@SiO_2 nanoparticles

The standard HeLa cell line derived from cervical cancer was used in this study. The HeLa cells were routinely cultured with DMEM (Dulbecco's modified eagle medium) containing 10% fetal calf serum (FCS). Cell cultures were kept at 37 °C in a humidified atmosphere containing 5% of CO_2. Cells were cultured in 6-well plate dishes (6 × 10 cm^2) at a density of 100 000 per plate. The cells were incubated with β-$NaYF_4$:20% Yb^{3+},2%Er^{3+} NPs without oleic acid (procedure describe in Section 2.4.1) and with β-$NaYF_4$:20%Yb^{3+},2%Er^{3+}@SiO_2 NPs. 291 μl of the sonicated initial aqueous colloidal suspension of β-$NaYF_4$:20%Yb^{3+},2%Er^{3+} NPs (3.44 mg ml^{-1}) was dissolved in 709 μl miliR water (the initial aqueous colloidal suspension of β-$NaYF_4$:20%Yb,2%Er@SiO_2 NPs contained 3.75 mg ml^{-1} and 267 μl of this sample was sonicated with 733 μl MiliR water to obtain 1 mg ml^{-1} concentration). Next, 2 μl of each diluted suspension was added to a 10 cm^2 dish with HeLa cells and incubated for 24 h. Then, the medium was changed to DMEM.[43]

2.6. Procedure of ligand-free β-$NaYF_4$:20%Yb^{3+},2%Er^{3+} nanoparticles preparation

Cyclohexane suspension of the NPs was precipitated by ethanol and washed by several cycles of sonication and centrifugation. Removal of oleic acid ligand took place through the using of different solution to dissolve NPs such as: HCl solution (0.1 M), acidic ethanol solution (pH 4), ethanol. Finally, the NPs were redispersed in 1 ml distilled water.[44,45]

2.7. Observation of β-$NaYF_4$:20%Yb^{3+},2%Er^{3+} and β-$NaYF_4$:20%Yb^{3+},2%Er^{3+}@SiO_2 nanoparticles inside the HeLa cells

The main technique for imaging both β-$NaYF_4$:20%Yb^{3+},2%Er^{3+} and β-$NaYF_4$:20%Yb^{3+},2%Er^{3+}@SiO_2 NPs was confocal microscopy, using a Zeiss 710 NLO system equipped with an infrared femtosecond laser (Coherent, Chameleon). The three channels were observed: the first, with excitation at 980 nm (femtosecond laser), was used for NP imaging in the 500–730 nm range; the second, with excitation at 705 nm (femtosecond laser), was used for imaging the nucleus marked by the Hoechst marker while detecting in the 425–475 nm range; the third, with excitation at 488 nm (continuous laser), was used to image the actine filaments build cell's cytoskeleton marked by antibodies labelled with fluorophore AlexaFluor 488 imaging with detection in the 495–572 nm range. This approach allows for imaging the marked structures and the UCNPs inside the selected cells.

Samples for confocal microscopy imaging were prepared according to the following procedure. Cells were inoculated onto 2 × 2 cm^2 slides and placed in the 6-well plate at 100 000 per plate. After 24 h incubation materials were separated by sonication and transfected as previously described (Section 2.4). Then, the medium was removed and the cells were washed twice with 2 ml of phosphate-buffered saline (PBS). Firstly, the cells were fixed by adding 2 ml of 3.7% formaldehyde in PBS and incubated for 20 min. After fixing, the cells were washed twice using 2 ml of PBS. Secondly, the cell's membrane was permeabilizated using 2 ml of 1% solution of TritonX-100 in 5% FBS/PBS (5% solution of Fetal Bovine Serum in PBS) and incubated for 10 min. Next, the cells were washed twice with 2 ml of PBS and permeabilization was blocked by adding 2 ml of 5% FBS/PBS and the samples were incubated for 30 min. Samples were washed with PBS and the cytoskeleton was stained with the primary rabbit actine antibody. 25 μl of the antibody in 5% FBS/PBS solution was dropped onto the slide with cells and covered with a capping slide. Samples were incubated for 1 h and then the capping slide was removed. The samples were washed twice using PBS. Using the same protocol the secondary antibody connected with AlexaFluor 488 was attached to the primary antibody. This step of preparation was conducted in dark to protect the fluorescent dye from photobleaching. The nucleus was marked using the Hoechst 33342 (25 μL) added.

2.8. Cytotoxicity of β-$NaYF_4$:20%Yb^{3+},2%Er^{3+} and β-$NaYF_4$:20%Yb^{3+},2%Er^{3+}@SiO_2 nanoparticles

The cytotoxicity of the β-$NaYF_4$:20%Yb^{3+},2%Er^{3+} and β-$NaYF_4$:20%Yb^{3+},2%Er^{3+}@SiO_2 NPs was evaluated by the MTT viability assay. The cells (10 000 per well) were incubated in each well of a 96-well plate with the β-$NaYF_4$:20%Yb^{3+},2%Er^{3+} and β-$NaYF_4$:20%Yb^{3+},2%Er^{3+}@SiO_2 NPs in the following concentrations: 0.1, 1, 5, 10 and 50 μg ml^{-1} in medium for 24 and 48 h. Following incubation, the cells were washed three times with the culture medium. Then, the MTT solution (5.0 mg ml^{-1}) was added. After incubation for another 4 h the MTT medium was removed from each well, DMSO was added and the mixture was shaken at room temperature to dissolve the reacted dye. The optical density (OD) was measured at 570 nm with a microplate reader. The cytotoxicity was calculated as follows: cytotoxicity = $(B \times 100\%)/A$, where A is the absorbance of the cells incubated with the culture medium (as a control) and B is the absorbance of the cells incubated with or without the NPs.

2.9. Transmission electron microscopy of the β-$NaYF_4$:20% Yb^{3+},2%Er^{3+} and β-$NaYF_4$:20%Yb^{3+},2%Er^{3+}@SiO_2 nanoparticles inside the HeLa cells

The presence of the NPs' inside the HeLa cells was confirmed by TEM imaging. Upon incubation with 1 μg ml^{-1} of β-$NaYF_4$:20% Yb^{3+},2%Er^{3+} or β-$NaYF_4$:20%Yb^{3+},2%Er^{3+}@SiO_2 NPs for 24 h HeLa cells pellets were fixed with 2% paraformaldehyde (Sigma

Aldrich, Germany) and 2.5% glutaraldehyde (Merck KGaA, Darmstadt, Germany) in 0.1 M cacodylate buffer, pH = 7.4 at 4 °C for 2 h, post-fixed with 1% osmium tetroxide (Sigma, USA) for 1 h, dehydrated in the graded series of ethanol (from 30% to 99.8%) and propylene oxide (ABCR GmbH, Germany), embedded in Agar 100 resin kit R1031 (Agar, USA) and polymerized at 60 °C for 24 h and sectioned (60 nm) using a RMC ultramicrotome (USA). The ultrathin sections were stained with uranyl acetate and lead citrate. Grids were examined with a JEM 1200EX electron microscope.

2.10. Reactive oxygen species generation by β-$NaYF_4$:20% Yb^{3+},0.2%Tm^{3+}@SiO_2 nanoparticles

The potential application of the presented nanoparticles to generate ROS was proved by electron paramagnetic resonance spectroscopy (EPR) after NIR light excitation. Water solution of NPs at 15 mg ml^{-1} concentration was mixed with spin trap buffer, as a spin trap used 1-hydroxy-3-methoxycarbonyl-2,2,5,5-tetramethylpyrrolidine (CMH), which shows EPR signal after reaction with the radicals.

The experiment was performed using as a near infrared sources: prototype LEDs system with maximum emission by 980 nm developed at University of Brasília, which worked with following parameters: 1 W cm^{-2} of power density, 30 minutes of irradiation (working cycle: 30 seconds of irradiation, 1 minute break). EPR signal was measured every ten minutes during 20 minutes of irradiation using Bruker EMX plus EPR spectrometer with X-Band using a 4119HS resonator with 5 G modulation, 200 G sweep width, and 20 mW microwave power. The ROS production was performed by spin trapping using by CMH cyclic hydroxylamine and Krebs Hepes buffer, with controlled time to air exposure to avoid false positives results.

3 Results and discussion

The structural properties and the phase purity of the β-$NaYF_4$:20%Yb^{3+},2%Er^{3+} and β-$NaYF_4$:20%Yb^{3+},0.2%Tm^{3+} UCNPs were examined by XRD measurements. The XRD patterns of the UCNPs are shown in Fig. 1. As can be observed the diffraction peaks of both NPs are well defined and the peak positions and intensities agree well with the values for the hexagonal $NaYF_4$ crystal.[7,46]

The size distribution of the UCNPs was determined by using XRD results and SEM images (Fig. 2a and b). From the line broadening of the (021) XRD peak of the samples β-$NaYF_4$:20% Yb^{3+},2%Er^{3+} and β-$NaYF_4$:20%Yb^{3+},0.2%Tm^{3+} and using the Debye–Scherrer formula an average crystallite size of 15.0 and 21.6 nm were calculated, respectively. Typical the UCNPs observed by SEM are well dispersed and very much uniform in size, with an average diameter of about 20.5 (±2.5) nm for the Er^{3+}-doped and 22.3 (±0.9) nm for the Tm^{3+}-doped NPs, as shown in the histograms presented in Fig. 2a and b. The average size values assessed from the SEM micrographs matched the average particle size obtained from the XRD data. Deviation in the average particle size obtained from the SEM and XRD data can be due to inaccuracy of the size estimation while using the XRD technique. The as-produced NPs have a regular spherical shape (Fig. 2), which is beneficial to their application in the cellular imaging.

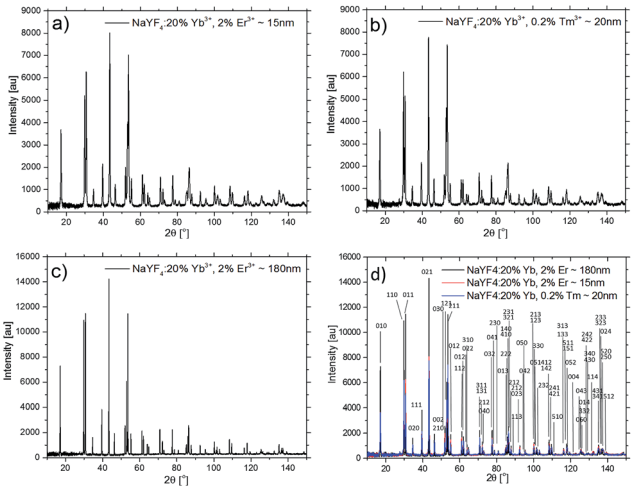

Fig. 1 XRD patterns of: (a) β-$NaYF_4$:20%Yb^{3+},2%Er^{3+} (~15 nm of diameter); (b) β-$NaYF_4$:20%Yb^{3+},0.2%Tm^{3+} (~20 nm); (c) β-$NaYF_4$:20% Yb^{3+},2%Er^{3+} (~180 nm) and (d) all diffractograms grouped together. Note that big crystals (c) were taken as reference.

The SiO_2-shell thickness and morphology of the β-$NaYF_4$:20%Yb^{3+},2%Er^{3+}@SiO_2 UCNPs were assessed by TEM. Typical TEM images of the NPs are shown in Fig. 2c. After coating with SiO_2, the average size of the Er^{3+}-doped NPs increased to about 24.6 (±3.7) nm. Nevertheless, after SiO_2-coating the shape and size monodispersity remained almost unchanged, as it observed on Fig. 2c, where the SiO_2-shell thickness is about 3.0 nm.

The EDX data are shown in Fig. 3. The EDX spectra confirm the presence of all elements (Na, Y, Yb, Er, F) in the β-$NaYF_4$:20%Yb^{3+},2%Er^{3+} and (Na, Y, Yb, Tm, F) in the β-$NaYF_4$:20%Yb^{3+},0.2%Tm^{3+} NPs (Fig. 3a and b). EDX maps show homogenous distribution of the elements forming the core and the shell of the NPs. Fig. 3c presents core, β-$NaYF_4$:20%Yb^{3+},2% Er^{3+} NPs and Fig. 3d shows the SiO_2 shell on the NPs.

The EDX data in Fig. 3 reviled homogeneous distribution of all elements in both types of the NPs. Likewise, a homogeneous elemental distribution is observed in the β-$NaYF_4$:20%Yb^{3+},2% Er^{3+}@SiO_2 NPs (see Fig. 3d). Silicon and oxygen are in the same location as other elements within the NPs. Indeed, silica forms a shell around the NPs which is visible in the Si EDX map in Fig. 3d. This finding confirms that the NPs were efficiently coated by SiO_2.

Before the cytotoxicity measurements of β-$NaYF_4$ NPs, the oleic acid was detached from the surface. Actually, the oleic acid acts as a surfactant capable to cap ligands while introducing the hydrophobic character to the NPs. Therefore, the oleic acid-coated UCNPs are not suitable for biological application, but can be easily removed out from the NP surface by HCl washing while the remaining functional groups associated with oleic acid can be identified by FT-IR spectroscopy (Fig. 4).

The oleic acid exhibits an IR band around 3430 cm^{-1}, corresponding to the hydroxyl group's stretching vibration. Two

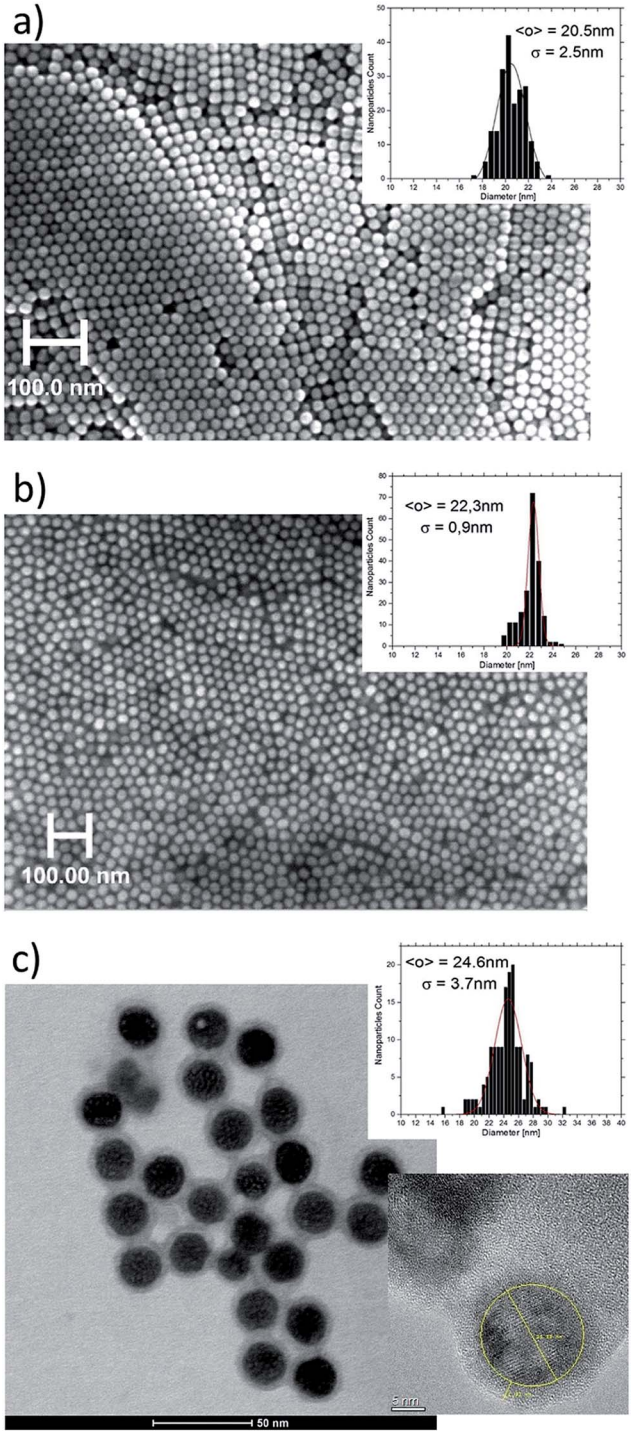

Fig. 2 SEM images of (a) β-$NaYF_4$:20%Yb^{3+},2%Er^{3+} NPs; (b) β-$NaYF_4$:20%Yb^{3+},0.2%Tm^{3+} NPs (inserts show particle size histograms obtained from 200 counting); (c) TEM image of β-$NaYF_4$:20%Yb^{3+},2%Er^{3+}@SiO_2 NPs (inserts show particle size histogram and HRTEM micrograph showing).

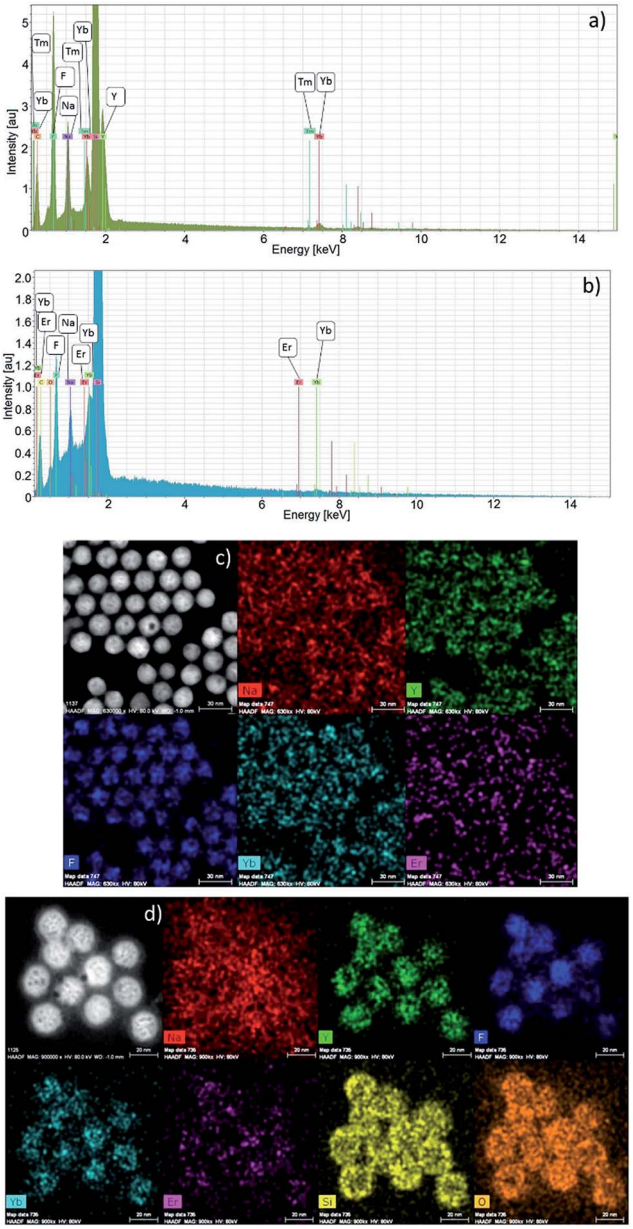

Fig. 3 EDX spectra of the (a) β-$NaYF_4$:20%Yb^{3+},0.2%Tm^{3+} and (b) β-$NaYF_4$:20%Yb^{3+},2%Er^{3+} NPs. EDX elemental distribution maps of the (c) β-$NaYF_4$:20%Yb^{3+},2%Er^{3+} NPs and (d) β-$NaYF_4$:20%Yb^{3+},2%Er^{3+}@SiO_2 NPs.

features peaking at 1632 and 1460 cm^{-1} are associated with the asymmetric and symmetric stretching vibrations of the carboxylic group (COO^-), respectively. The two peaks at 2924 and 2854 cm^{-1} can be assigned to the asymmetric and symmetric stretching vibrations of methylene group, respectively. As shown in Fig. 4, after the HCl purification, the quenching of the features in the FT-IR spectrum in the 4000–1000 cm^{-1} range indicates that the pure (oleic acid free) $NaYF_4$:20%Yb^{3+},2%Er^{3+} NPs were obtained.

The upconversion spectra of 1 mg ml^{-1} suspensions of β-$NaYF_4$:20%Yb^{3+},2%Er^{3+} and β-$NaYF_4$:20%Yb^{3+},0.2%Tm^{3+} NPs in cyclohexane under 980 nm laser diode excitation (power density 12.14 W cm^{-2}) are shown in Fig. 5a and d. The insets of Fig. 5a and d show a digital photograph of the total upconversion luminescence of the same solution under the described excitation condition.

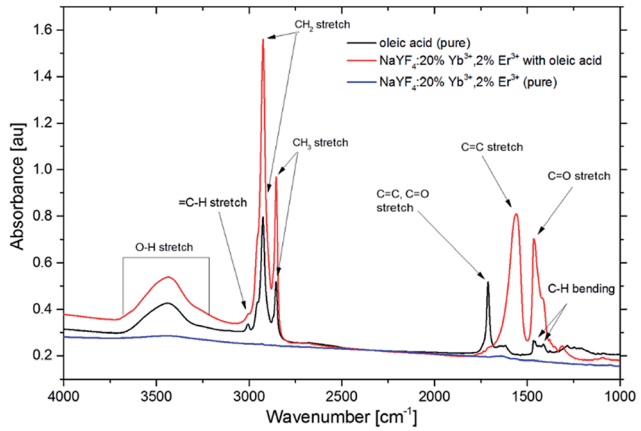

Fig. 4 FT-IR spectra of oleic acid, β-$NaYF_4$:20%Yb^{3+},2%Er^{3+} NPs with oleic acid and β-$NaYF_4$:20%Yb^{3+},2%Er^{3+} NPs after HCl washing.

In order to determine the number of photons responsible for the upconversion mechanism the intensity of the upconversion emission (UCL) was recorded as a function of the 980 nm excitation (Fig. 5c and f).

Stable suspension of the NPs in aqueous medium is very important for effective bioimaging applications. Therefore, for the biological applications the silica-coated NPs (β-$NaYF_4$:20% Yb^{3+},2%Er^{3+}@SiO_2) were produce. As a result of surface modification the β-$NaYF_4$:20%Yb^{3+},2%Er^{3+}@SiO_2 NPs are stable in water and emit strong upconverting fluorescence (Fig. 5b and e).

The emission bands of the β-$NaYF_4$:20%Yb^{3+},2%Er^{3+} and the β-$NaYF_4$:20%Yb^{3+},0.2%Tm^{3+} NPs after NIR light excitation are shown in Fig. 5a and d. They can be assigned to the transitions between the 4f–4f levels of the Er^{3+} and Tm^{3+} ions. The spectrum of the β-$NaYF_4$:20%Yb^{3+},2%Er^{3+} NPs (see Fig. 5a) exhibits three emission bands. The two strong green emissions at 540 and 550 nm originate from the $^2H_{11/2}$ to $^4I_{15/2}$ and from $^4S_{3/2}$ to $^4I_{15/2}$ transitions, respectively. The red emission at 654 nm can be assigned to the transition from $^4F_{9/2}$ to $^4I_{15/2}$ levels.[47,48]

Four Tm^{3+} emission bands were observed in the β-$NaYF_4$:20%Yb^{3+},0.2%Tm^{3+} NPs (Fig. 5d) with maximum position of peaks at 474, 645, 697 and 800 nm.

In order to determine the number of photons responsible for the upconversion mechanism, the intensity of the upconversion luminescence (UCL) was recorded as a function of the power of 980 nm excitation (see Fig. 5c and f). The UCL intensity (I_{up}) in the lanthanide-doped UCNPs depends on the laser power (P) excitation. This dependence can be expressed as: $I_{up} \sim P^n$, where n describes the quantity of absorbed photons in the luminescence process. Fig. 5c shows the green and red Er^{3+} upconversion emission intensities in quadratic power dependence at low excitation, indicating the two-photon upconversion mechanisms. For the Tm^{3+}-doped NPs (see Fig. 5f) three- and two-photon power dependencies were observed for the $^1G_4$ to $^3H_6$ and $^3H_4$ to $^3H_6$ emissions. Similar observation has been reported previously in the literature.[47]

The upconversion mechanisms for the Er^{3+}/Yb^{3+} and Tm^{3+}/Yb^{3+} ion couples within the β-$NaYF_4$ crystal are well-known[49]

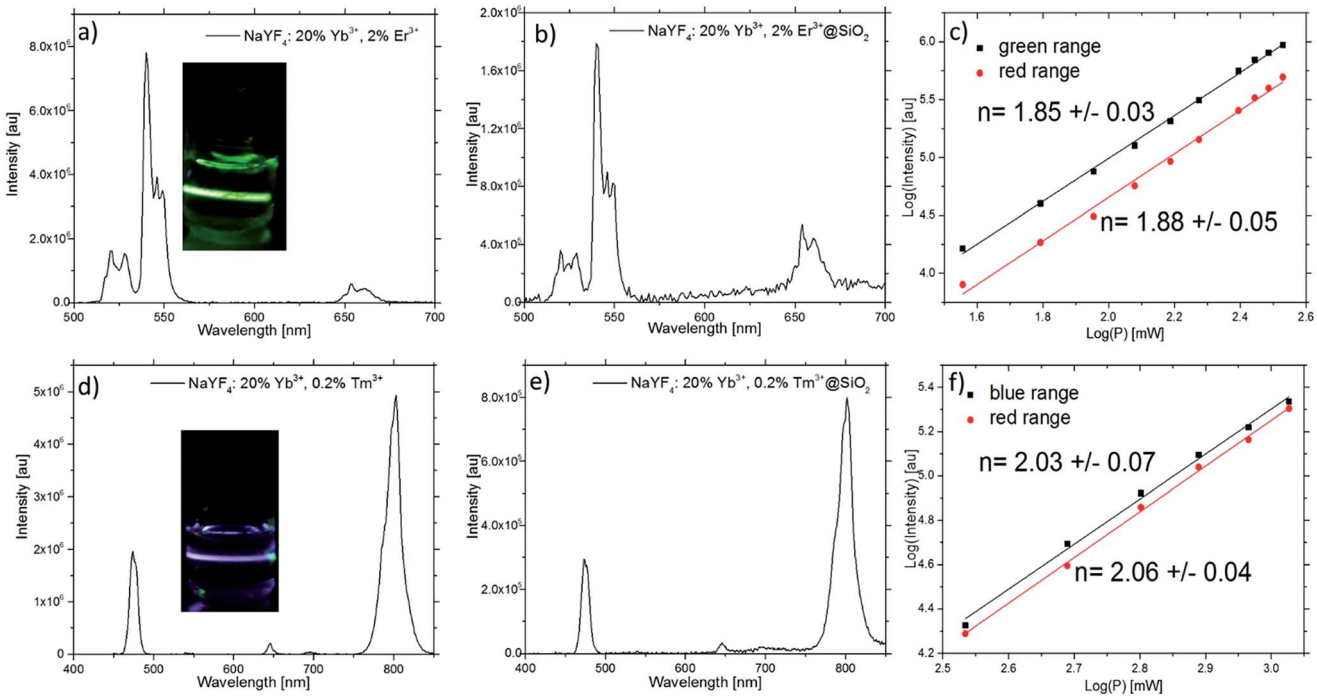

Fig. 5 Luminescence spectra of the NPs suspensions (1 mg ml^{-1}) in cyclohexane excited with a 980 nm laser diode (power density 12.14 W cm^{-2}): (a) β-$NaYF_4$:20%Yb^{3+},2%Er^{3+}, (d) β-$NaYF_4$:20%Yb^{3+},0.2%Tm^{3+} and 1 mg ml^{-1} in water suspension of (b) β-$NaYF_4$:20%Yb^{3+},2%Er^{3+}@SiO_2 aand (e) β-$NaYF_4$:20%Yb^{3+},0.2%Tm^{3+}@SiO_2 NPs excited with a 980 nm laser diode (power density 12.14 W cm^{-2}). Double log plot of power dependence of the upconverted emissions of 1 mg ml^{-1} suspensions of the NPs in cyclohexane excited at 980 nm: (c) β-$NaYF_4$:20%Yb^{3+},2%Er^{3+} and (f) β-$NaYF_4$:20%Yb^{3+},0.2%Tm^{3+}. Symbols are experimental data while the straight lines are least-squares fits to the data points.

and schematically represented in Fig. 6. In the case of β-$NaYF_4$:20%Yb^{3+},2%Er^{3+} the excitation energy is transferred from the Yb^{3+} ion in the $^2F_{5/2}$ state to the Er^{3+} ion in the $^4I_{11/2}$ state. The second energy transfer from the Yb^{3+} ion can populate the $^4F_{7/2}$ state of the Er^{3+} ion. The Er^{3+} ion can relax non-radiative (without emission of photons) to the $^2H_{11/2}$ and $^4S_{3/2}$ levels before emitting green light *via* $^2H_{11/2} \rightarrow {}^4I_{15/2}$ and $^4S_{3/2} \rightarrow {}^4I_{15/2}$ transitions. Alternatively, the Er^{3+} ion can relax and populate the $^4F_{9/2}$ level, leading to the red $^4F_{9/2} \rightarrow {}^4I_{15/2}$ emission. The $^4F_{9/2}$ level may also be populated from the $^4I_{13/2}$ level of the Er^{3+} ion by absorption of a 980 nm photon, or by energy transfer from an Yb^{3+} ion, with the $^4I_{13/2}$ state being initially populated *via* the non-radiative $^4I_{11/2} \rightarrow {}^4I_{13/2}$ relaxation.[47]

Nanoparticles doped by Tm^{3+} ions are characterized by four main emission bands (see Fig. 5d) with wavelength 474, 645, 697 and 800 nm. After absorption of 980 nm by Yb^{3+} ions, energy is transferred from $^2F_{5/2}$ ytterbium state to $^3H_6$, $^3H_5$, $^3F_2$ and $^1G_4$ states, respectively. In consequence of energy transfers and non-radiative transitions between the levels followed the emission from states: $^1G_4 \rightarrow {}^3H_6$, $^1G_4 \rightarrow {}^3F_4$, $^3F_3 \rightarrow {}^3H_6$ and $^3H_4 \rightarrow {}^3H_6$ respectively. These emission bands are described above (Fig. 6).[52,53]

As shown in Fig. 5a and e presence of the SiO_2 shell, has an impact to the physical aspect of the luminescence. Analysis of the core $NaYF_4$:20%Yb^{3+},2%Er^{3+} NPs emission spectrum points to the higher luminescence intensity of the green area compared to the red area. The ratio of the two luminescence areas has different characteristic for the NPs coated by SiO_2. In this material the intensity of the green luminescence is lower than the red. This difference is due to the modification of the NPs surface which offsets the surface effects and contribute to the energy of phonons relaxation, which takes part in the upconversion, as we reported previously.[54] The silicon oxide shell enhances the non-radiative decay which causes higher quantity of the radiative emission from $^4F_{9/2}$ level than $^4S_{3/2}$ level (see Fig. 6).

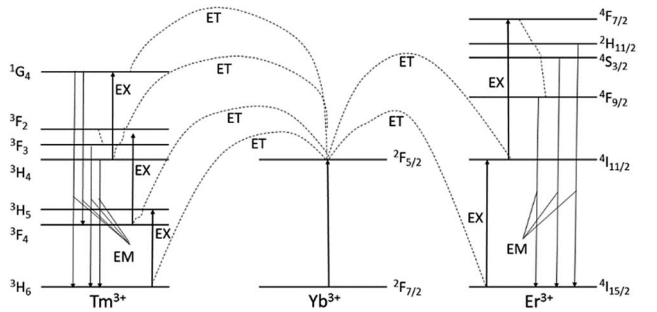

Fig. 6 The energy level diagrams of the Er^{3+}, Tm^{3+} and Yb^{3+} dopant ions and the corresponding upconversion mechanisms under 980 nm excitation. The ET interrupted arrows represent energy transfer (non-radiative transition), EX – excitation and EM – emission of visible photons (radiative transition).[51–53]

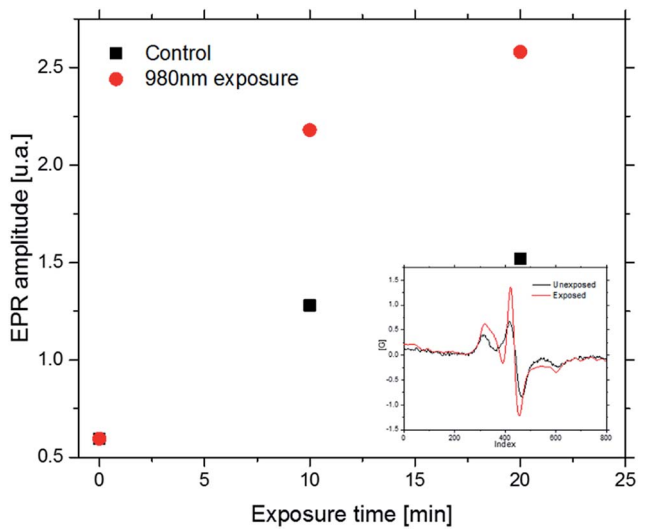

Fig. 7 EPR spectroscopy graph of CMH signal. Spin trap was activated by reactive oxygen species from decomposition of water by NPs emitted high energy light. Control group shows non irradiated solution. Tested group was irradiated during 30 minutes with 980 nm NIR sources at 1 W cm^{-2} power density, respectively by LEDs system. Insert shows example spectrum (after 20 minute of irradiation) using to make a graph.

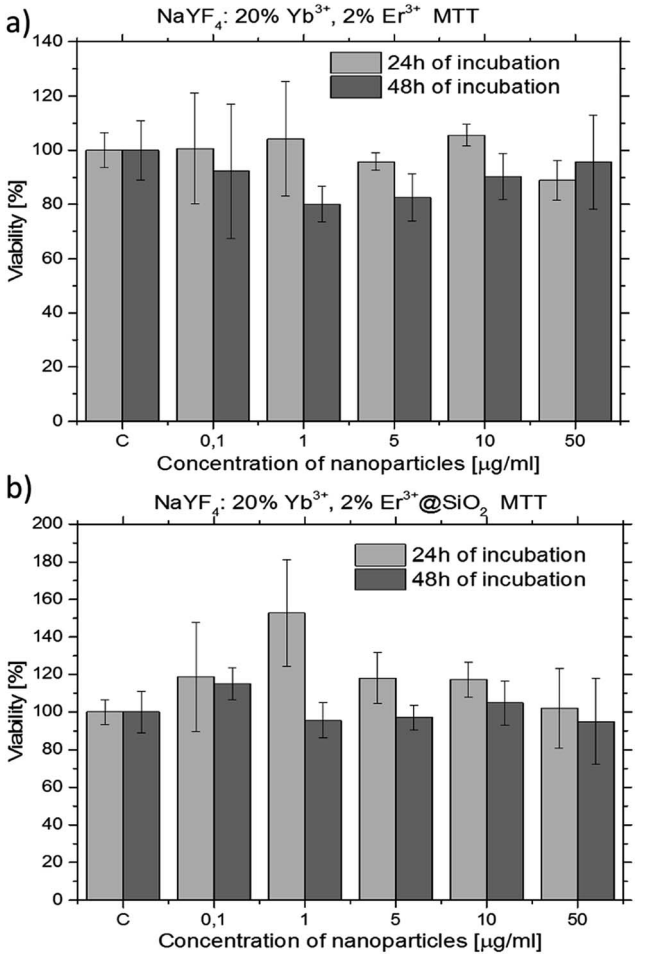

Fig. 8 Cell viability values estimated from the MTT assay *versus* concentration of the β-$NaYF_4$:20%Yb^{3+},2%Er^{3+} NPs without oleic acid (a) and β-$NaYF_4$:20%Yb^{3+},2%Er^{3+}@SiO_2 NPs (b). Cells were incubated with 0–50 μg ml^{-1} of the NPs at 37 °C, for 24 h (a, c) and 48 h (b, d). Each data point is represented as mean (SD from 4 trials).

We have synthesized and characterized β-$NaYF_4$:20% Yb^{3+},0.2%Tm^{3+}@SiO_2 nanoparticles exhibiting several promising properties useful in medical applications: bio imagining of cells and tissues and modern PDT. A high efficiency NIR upconversion and, due to presence of Tm^{3+}–Yb^{3+} pair ions, ROS generation capability, renders the SiO_2 shell coated nanoparticles to become potentially useful theranostic agent.

The experiment, performed under standard conditions, was aimed to test the possibility of β-$NaYF_4$:20%Yb^{3+},0.2% Tm^{3+}@SiO_2 NPs to generate ROS without any additional organic molecules. Comparison of the control sample-without the LED irradiation and the NPs suspension exposed to the light, shows enhanced level of the CMH spin trap signal. Intensity of the EPR signals for the control and LED illuminated samples were summarized (Fig. 7). We observed the 70% increased in the EPR signal after 10 min of irradiation and 70% after 20 min of irradiation. The ROS generation from Tm-doped nanoparticles is potentially promising for the future PDT therapy.

In order to investigate the cytotoxicity of both β-$NaYF_4$:20% Yb^{3+},2%Er^{3+} (without oleic acid) and β-$NaYF_4$:20%Yb^{3+},2% Er^{3+}@SiO_2 NPs a MTT assay, using HeLa cell line, was performed to determine the effect of the UCNPs on the cell proliferation after 24 and 48 h (Fig. 8).

One of the most important aspect in the design and the synthesis of biomarkers is their toxicity. In order to investigate the cytotoxicity of β-$NaYF_4$:20%Yb^{3+},2%Er^{3+} (without oleic acid) and β-$NaYF_4$:20%Yb^{3+},2%Er^{3+}@SiO_2 NPs a MTT assay was used. No significant difference in the cell proliferation was observed in the absence or presence of 0.1–50 μg ml^{-1} UCNPs (see Fig. 8). The cellular viabilities were estimated to be greater than 90% after 24 h and 80% after 48 h for the β-$NaYF_4$:20%Yb^{3+},2%Er^{3+} NPs (Fig. 8a) and almost 100% after 24 and 48 h for the β-$NaYF_4$:20%Yb^{3+},2%Er^{3+}@SiO_2 NPs (Fig. 8b). These data show that the β-$NaYF_4$:20%Yb^{3+},2%Er^{3+} NPs have relatively low cytotoxicity after 24 and 48 h of incubation even at relatively high concentration (50 μg ml^{-1}). The β-$NaYF_4$:20%Yb^{3+},2% Er^{3+}@SiO_2 NPs have no apparent cytotoxicity (after 48 h of incubation, the cellular viabilities were 100% even at the NPs concentration of 50 μg ml^{-1}).

Cellular uptake of both β-$NaYF_4$:20%Yb^{3+},2%Er^{3+} (without oleic acid) and β-$NaYF_4$:20%Yb^{3+},2%Er^{3+}@SiO_2 NPs by HeLa cells was visualized by multiphoton confocal imaging (Fig. 9a and b). Cells stained by the NPs were exposed to 980 nm irradiation using a femtosecond Ti:sapphire pulsed laser while their typical upconversion luminescence was measured in 500–730 nm channel for the green and red emissions. In addition, the cytoskeleton of the HeLa cells was stained by the antibodies conjugated with the AlexaFluor 488 for a better visualization of the cells. The blue color indicates the nucleus stained by Hoechst 33342 channel (excitation: 705 nm – femtosecond

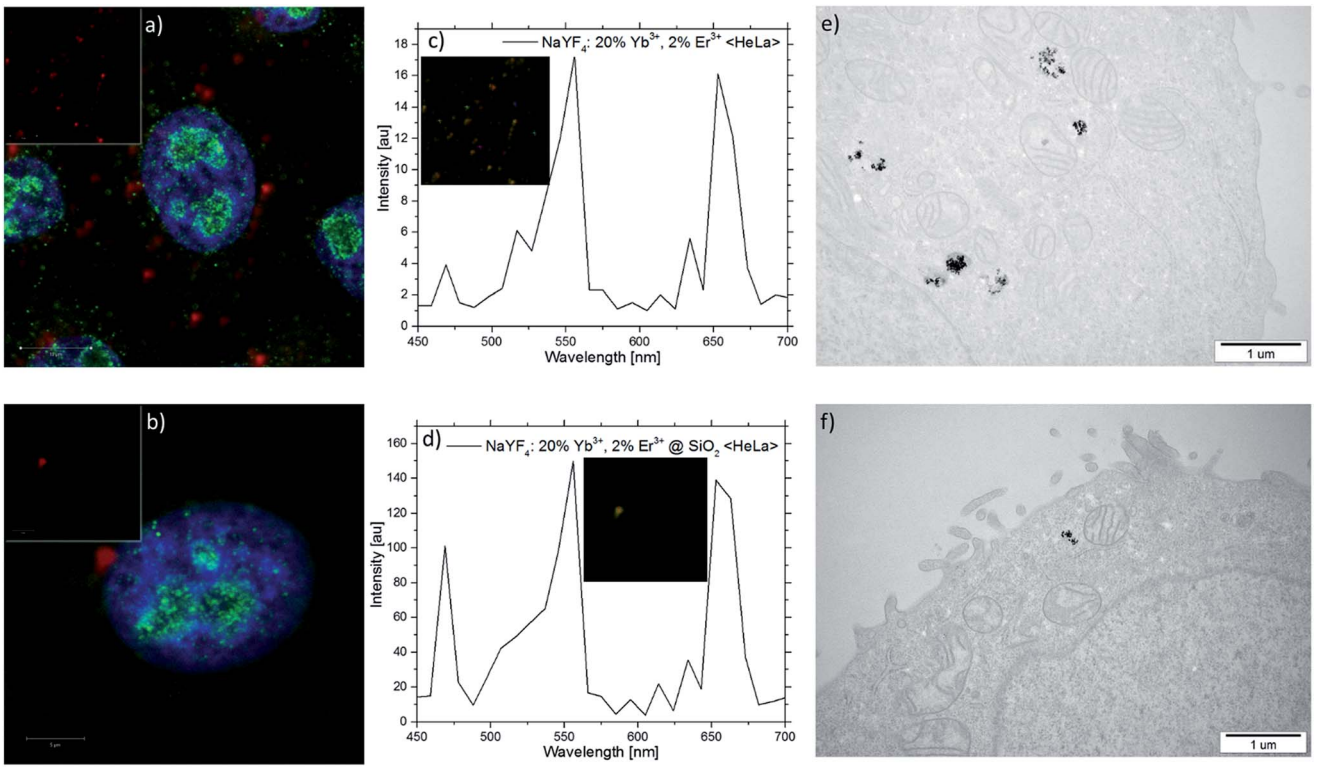

Fig. 9 Confocal images of the HeLa cells incubated with the (a) β-$NaYF_4$:20%Yb^{3+},2%Er^{3+} and (b) β-$NaYF_4$:20%Yb^{3+},2%Er^{3+}@SiO_2 NPs after 24 h of incubation with 0.001 mg ml^{-1} of the NPs concentration. The insets in the panels (a) and (b) show the upconversion channels. Luminescence spectra of the (c) β-$NaYF_4$:20%Yb^{3+},2%Er^{3+} and (d) β-$NaYF_4$:20%Yb^{3+},2%Er^{3+}@SiO_2 NPs inside the HeLa cells excited with the 980 nm wavelength light at 1.11 W μm^{-2} laser power. Insets in (c) and (d) show images with luminescent spots. TEM images showing the (e) β-$NaYF_4$:20% Yb^{3+},2%Er^{3+} and (f) β-$NaYF_4$:20%Yb^{3+},2%Er^{3+}@SiO_2 NPs within HeLa cells (incubation with 1 μg ml^{-1} of NPs at 37 °C, for 24 h).

laser, power density: 0.72 W μm^{-2}, detection: 425–475 nm). Green color indicates the actine cytoskeleton filaments marked by the antibody labeled with AlexaFluor 488 (excitation: 488 nm – CW, power density: 0.0375 W μm^{-2}, detection: 495–572 nm). Red color indicates the UCNPs channel (excitation: 980 nm – femtosecond laser, power density: 1.11 W μm^{-2}; detection: 500–730 nm). A spectrum recorded from the cells showed that the luminescence exhibits two emission bands, with maxima at 556 and 653 nm after 980 nm of excitation (Fig. 9c and d). Fig. 9e and f shows the TEM images of (e) SiO_2-uncoated and (f) SiO_2-coated NPs (without oleic acid) inside the HeLa cells.

The overlay of the upconversion channel and cytoskeleton channel indicate that the UCL signal distributions are strongly correlated with the cytoskeleton of HeLa cells, meaning that the NPs spontaneously enter into the cells and locate within the cytoplasm. In contrast, the HeLa cells incubated with the β-$NaYF_4$:20%Yb^{3+},2%Er^{3+}@SiO_2 NPs (Fig. 9b) show weaker luminescence in the upconverting green channel under the same conditions, suggesting a lower uptake by the HeLa cells. This may be due to differences in the NP surface charge. The spectrum recorded from the HeLa cells shows that the luminescence exhibits two characteristic emission bands, with maxima at 556 and 653 nm (Fig. 9d).

It should be pointed out that no measurable autofluorescence signal was observed after 980 nm excitation in the upconverting channel of the HeLa cells labelled with both β-$NaYF_4$:20%Yb^{3+},2%Er^{3+} and β-$NaYF_4$:20%Yb^{3+},2%Er^{3+}@SiO_2 NPs (insets of Fig. 9a and b). Moreover, in the upconverting channel a high signal-to-noise ratio, with relatively high upconversion intensity, was observed and no background fluorescence was noted. As far as the biological imaging is concerned, the finding is an interesting and useful feature of the UCNPs,[50] which has not been obtained in the traditional single-photon or two-photon fluorescent imaging.[55–66] While excited with the 980 nm laser light the biological samples presented weak absorption with no luminescence in the visible region. Fig. 9e and f shows that SiO_2-coated and SiO_2-uncoated NPs (without oleic acid) were trapped within cytosolic vesicular structures after being up-taken by the HeLa cells, suggesting that the NPs' cellular internalization took place by endocytosis in both cases.

4 Conclusions

The present report describes a successful synthesis and characterization of the β-$NaYF_4$:20%Yb^{3+},2%Er^{3+} and β-$NaYF_4$:20%Yb^{3+},0.2%Tm^{3+} NPs. Under NIR light irradiation the β-$NaYF_4$:20%Yb^{3+},2%Er^{3+} NPs exhibited intense green and red luminescence while the β-$NaYF_4$:20%Yb^{3+},0.2%Tm^{3+} NPs exhibited intense ultra-violet, blue and red luminescence. UV emission range is capable to generate reactive oxygen species in aqueous environment. Compared to traditionl therapies based on ROS generation, we presented materials which could generate ROS without any other components attached to the nanoparticles. This property allows to solve a common problems with traditional systems containing photosensitizers (photobleaching, dose limitation). The synthesized core NPs were surface coated with silica, having the silica shell thickness about 3 nm. The nanoparticle's core/shell morphology, its structure and surface modification were confirmed by XRD, TEM, SEM, EDX, and FTIR measurements. All synthesized nanomaterials formed stable aqueous colloids exhibiting green or blue luminescence under NIR laser irradiation (λ_{ex} = 980 nm). The cytotoxicity assays revealed that all the prepared nanomaterials are relatively nontoxic even in relatively high concentration (50 μg ml^{-1}) for 48 h incubation. The β-$NaYF_4$:20%Yb^{3+},2%Er^{3+} and β-$NaYF_4$:20%Yb^{3+},2%Er^{3+}@SiO_2 NPs were visualised inside the cytoplasm of HeLa cells. Moreover, no apparent background fluorescence was observed inside the HeLa cells after the NIR light excitation with the strong upconversion of the nanoparticles. Our report shows several promising applications of the inorganic, lanthanide-doped nanophosphors, in particularly, as potential biomarkers, contrast agents, and drug-delivery systems.

Acknowledgements

This research was partially supported by the EU within the European Regional Development Fund, through the grant Innovative Economy (POIG.01.01.02-00-008/08), the project 'Development of the cluster center of biomedical engineering' implemented under the Economy Operational Program (project no. UDA-POIG.05.01.00-00), the EU Research Project FP7-People-2012-IRSES-BRASINOEU (Grant Agreement Number: PIRSES-GA-2012-318916), the grants of PNSC 2013/11/B/NZ1/00089, NN UMO-2013/08/A/ST3/00297, DEC-2012/07/B/ST5/02080, and DEC-2014/15/D/ST5/02604. This work has been done in the NanoFun laboratories co-financed by the European Regional Development Fund within the Innovation Economy Operational Program (Project No. POIG.02.02.00-00-025/09). This research was also co-financed by the Swiss National Science Foundation through the Nano-Tera.ch Focused Project (NTF), 'NanoUp'. The use of the FEI Tecnai Osiris TEM instrument located at the Facility for Electron Microscopy & Sample Preparation of the University of Rzeszow is acknowledged.

Notes and references

1 R. A. Jalil and Y. Zhang, Biocompatibility of Silica Coated NaYF4 Upconversion Fluorescent Nanocrystals, *Biomaterials*, 2008, **29**, 4122–4128.
2 Q. L. DeChermont, C. Chaneac, J. Seguin, F. Pelle, S. Maıtrejean, J. P. Jolivet, D. Gourier, M. Bessodes and D. Scherman, Nanoprobes with Near-Infrared Persistent Luminescence for In Vivo Imaging, *Proc. Natl. Acad. Sci. U. S. A.*, 2007, **104**, 9266–9271.
3 J. L. West and N. J. Halas, Engineered Nanomaterials for Biophotonics Applications: Improving Sensing, Imaging and Therapeutics, *Annu. Rev. Biomed. Eng.*, 2003, **5**, 285–292.
4 M. S. Gee, R. Upadhyay, H. Bergquist, H. Alencar, F. Reynolds, M. Maricevich, R. Weissleder, L. Josephson and U. Mahmood, Human Breast Cancer Tumor Models: Molecular Imaging of Drug Susceptibility and Dosing During HER2/Neu-Targeted Therapy, *Radiology*, 2008, **248**, 925–935.

5 F. Auzel, Upconversion and Anti-Stokes Processes with f and d Ions in Solids, *Chem. Rev.*, 2004, **104**, 139–173.
6 X. Wang and Y. D. Li, Monodisperse Nanocrystals: General Synthesis, Assembly, and Their Applications, *Chem. Commun.*, 2007, **28**, 2901–2910.
7 M. Wang, C.-C. Mi, W.-X. Wang, C.-H. Liu, Y.-F. Wu, Z.-R. Xu, C.-B. Mao and S.-K. Xu, Immunolabeling and NIR-Excited Fluorescent Imaging of HeLa Cells by Using NaYF4:Yb, Er Upconversion Nanoparticles, *ACS Nano*, 2009, **3**(6), 1580–1586.
8 J. W. Zhao, Y. J. Sun, X. G. Kong, L. J. Tian, Y. Wang, L. P. Tu, J. L. Zhao and H. Zhang, Controlled Synthesis, Formation Mechanism, and Great Enhancement of Red Upconversion Luminescence of NaYF4:Yb3,Er3 Nanocrystals/Submicroplates at Low Doping Level, *J. Phys. Chem. B*, 2008, **112**, 15666–15672.
9 S. Heer, K. Kompe, H. U. Gudel and M. Haase, Highly Efficient Multicolour Upconversion Emission in Transparent Colloids of Lanthanide-Doped NaYF4 Nanocrystals, *Adv. Mater.*, 2004, **16**, 2102–2105.
10 O. Ehlert, R. Thomann, M. Darbandi and T. Nann, A Four-Color Colloidal Multiplexing Nanoparticle System, *ACS Nano*, 2008, **2**, 120–124.
11 H. Kolarova, P. Nevrelova, K. Tomankova, P. Kolar, R. Bajgar and J. Mosinger, Production of reactive oxygen species after photodynamic therapy by porphyrin sensitizers, *Gen. Physiol. Biophys.*, 2008, **27**, 101–105.
12 X.-F. Qiao, J.-C. Zhou, J.-W. Xiao, Ye-F. Wang, L.-D. Sun and C.-H. Yan, Triple-functional core–shell structured upconversion luminescent nanoparticles covalently grafted with photosensitizer for luminescent, magnetic resonance imaging and photodynamic therapy in vitro, *Nanoscale*, 2012, **4**, 4611–4623.
13 Y. Guo, S. Rogelj and P. Zhang, Rose Bengal-decorated silica nanoparticles as photosensitizers for inactivation of gram-positive bacteria, *Nanotechnology*, 2010, **21**, 065102.
14 G. S. Yi and G. M. Chow, Synthesis of Hexagonal-Phase NaYF4: Yb, Er and NaYF4:Yb, Tm Nanocrystals with Efficient Up- Conversion Fluorescence, *Adv. Funct. Mater.*, 2006, **16**, 2324–2329.
15 Y. Wei, F. Q. Lu, X. R. Zhang and D. P. Chen, Synthesis of Oil-Dispersible Hexagonal-Phase and Hexagonal-Shaped NaYF4:Yb,Er Nanoplates, *Chem. Mater.*, 2006, **18**, 5733–5737.
16 L. Y. Wang and Y. D. Li, Controlled Synthesis and Luminescence of Lanthanide Doped NaYF4 Nanocrystals, *Chem. Mater.*, 2007, **19**, 727–734.
17 H. C. Lu, G. S. Yi, S. Y. Zhao, D. P. Chen, L. H. Guo and J. Cheng, Synthesis and Characterization of Multi-Functional Nanoparticles Possessing Magnetic, Up-Conversion Fluorescence and Bio-Affinity Properties, *J. Mater. Chem.*, 2004, **14**, 1336–1341.
18 F. Wang and X. G. Liu, Advances in the chemistry of lanthanide-doped upconversion nanocrystals, *Chem. Soc. Rev.*, 2009, **38**, 976–989.
19 G. K. Das, B. C. Heng, S. C. Ng, T. White, J. S. C. Loo, L. D'Silva, P. Padmanabhan, K. K. Bhakoo, S. T. Selvan and T. T. Y. Tan, Gadolinium oxide ultranarrow nanorods as multimodal contrast agents for optical and magnetic resonances imaging, *Langmuir*, 2010, **26**, 8959–8965.
20 D. K. Yi, S. T. Selvan, S. S. Lee, G. G. Papaefthymiou, D. Kundaliya and J. Y. Ying, Silica-coated nanocomposites of magnetic nanoparticles and quantum dots, *J. Am. Chem. Soc.*, 2005, **127**, 4990–4991.
21 Z. Y. Liu, G. S. Yi, H. T. Zhang, J. Ding, Y. W. Zhang and X. Min, Monodisperse silica nanoparticles encapsulating upconversion fluorescent and superparamagnetic nanocrystals, *Chem. Commun.*, 2008, 694–696.
22 F. Zhang, G. B. Braun, A. Pallaoro, Y. Zhang, Y. Shi, D. Cui, M. Moskovits, D. Zhao and G. D. Stucky, Mesoporous Multifunctional Upconversion Luminescent and Magnetic "Nanorattle" Materials for Targeted Chemotherapy, *Nano Lett.*, 2012, **12**, 61–67.
23 H. Ow, D. R. Larson, M. Srivastava, B. A. Baird, W. W. Webb and U. Wiesner, Bright and stable core-shell fluorescent silica nanoparticles, *Nano Lett.*, 2005, **5**, 113–117.
24 L. M. Rossi, L. Shi, F. H. Quina and Z. Rosenzweig, Stober synthesis of monodispersed luminescent silica nanoparticles for bioanalytical assays, *Langmuir*, 2005, **21**, 4277–4280.
25 A. Gnach, T. Lipinski, A. Bednarkiewicz, J. Rybka and J. A. Capobianco, Upconverting nanoparticles: assessing the toxicity, *Chem. Soc. Rev.*, 2015, **44**, 1561.
26 S. Sivakumar, P. R. Diamente and F. C. J. M. van Veggel, Silica-Coated Ln3+-Doped LaF3 NanoparticlesasRobus t Down- and Upconverting Biolabels, *Chem.–Eur. J.*, 2006, **12**, 5878–5884.
27 F. Wang, X. Yang, L. Ma, B. Huang, N. Na, Y. E, D. He and J. Ouyang, Multifunctional up-converting nanocomposites with multimodal imaging and photosensitization at near-infrared excitation, *J. Mater. Chem.*, 2012, **22**, 24597–24604.
28 K. Liu, X. Liu, Q. Zeng, Y. Zhang, L. Tu, T. Liu, *et al.*, Covalently Assembled NIR Nanoplatform for Simultaneous Fluorescence Imaging and Photodynamic Therapy of Cancer Cells, *ACS Nano*, 2012, **6**(5), 4054–4062.
29 C. Wang, L. Cheng and Z. Liu, Upconversion Nanoparticles for Photodynamic Therapy and Other Cancer Therapeutics, *Theranostics*, 2013, **3**(5), 317–330.
30 M. T. Jarvi, M. S. Patterson and B. C. Wilson, Insights into Photodynamic Therapy Dosimetry: Simultaneous Singlet Oxygen Luminescence and Photosensitizer Photobleaching Measurements, *Biophys. J.*, 2012, **102**(3), 661–671.
31 S. Tan, P. Yang, N. Niu, S. Gai, J. Wang, X. Jing and J. Lin, Monodisperse and core–shell structured NaYF4:Ln@SiO2 (Ln = Yb/Er, Yb/Tm) microspheres: Synthesis and characterization, *J. Alloys Compd.*, 2010, **490**, 684–689.
32 J. W. Stouwdam and F. C. J. M. van Veggel, Near-infrared emission of redispersible Er3+, Nd3+ and Ho3+ doped LaF3 nanoparticles, *Nano Lett.*, 2002, **2**, 733–737.
33 J. W. Stouwdam and F. C. J. M. van Veggel, Improvement in the Luminescence Properties and Processability of LnF3/Ln and LnPO4/Ln Nanoparticles by Surface Modification, *Langmuir*, 2004, **20**, 11763–11771.
34 V. Sudarsan, F. C. J. M. van Veggel, R. A. Herring and M. Raudsepp, Surface Eu3+ ions are different than "bulk"

Eu3+ ions in crystalline doped LaF3 nanoparticles, *J. Mater. Chem.*, 2005, **15**, 1332–1342.

35 F. Vetrone, J. C. Boyer, J. A. Capobianco, A. Speghini and A. M. Bettinelli, Effect of Yb3+ Codoping on the Upconversion Emission in Nanocrystalline Y2O3:Er3+, *J. Phys. Chem. B*, 2003, **107**, 1107–1112.

36 A. Patra, C. S. Friend, R. Kapoor and P. N. Prasad, Effect of crystal nature on upconversion luminescence in Er3+:ZrO2 nanocrystals, *Appl. Phys. Lett.*, 2003, **83**, 284–286.

37 S. Heer, K. Kompe, H.-U. Gudel and M. Haase, Highly efficient multicolour upconversion emission in transparent colloidal of nanoparticle-doped NaYF4 nanocrystals, *Adv. Mater.*, 2004, **16**, 2102–2105.

38 M. H. V. Werts, R. T. F. Jukes and J. W. Verhoeven, The emission spectrum and the radiative lifetime of Eu3+ in luminescent lanthanide complexes, *Phys. Chem. Chem. Phys.*, 2002, **4**, 1542–1548.

39 K. Binnemans, R. Van Deun, C. Gorller-Walrand and J. L. Adam, Spectroscopic properties of trivalent lanthanide ions in fluorophosphates glasses, *J. Non-Cryst. Solids*, 1998, **238**, 11–29.

40 J. E. Roberts, Lanthanum and Neodymium Salts of Trifluoroacetic Acid, *J. Am. Chem. Soc.*, 1961, **83**, 1087.

41 H.-X. Mai, Ya-W. Zhang, R. Si, Z.-G. Yan, L.-D. Sun, Li-P. You and C.-H. Yan, High-Quality Sodium Rare-Earth Fluoride Nanocrystals: Controlled Synthesis and Optical Properties, *J. Am. Chem. Soc.*, 2006, **128**, 6426–6436.

42 X.-F. Qiao, J.-C. Zhou, J.-W. Xiao, Ye-F. Wang, L.-D. Sun and C.-H. Yan, Triple-functional core–shell structured upconversion luminescent nanoparticles covalently grafted with photosensitizer for luminescent, magnetic resonance imaging and photodynamic therapy in vitro, *Nanoscale*, 2012, **4**, 4611.

43 B. Sikora, K. Fronc, I. Kamińska, K. Koper, S. Szewczyk, B. Paterczyk, T. Wojciechowski, K. Sobczak, R. Minikayev, W. Paszkowicz, P. Stępień and D. Elbaum, Transport of NaYF4:Er3C, Yb3C up-converting nanoparticles into HeLa cells, IOP Publishing, *Nanotechnology*, 2013, **24**, 235702.

44 F. Wang, R. Deng, J. Wang, Q. Wang, Y. Han, H. Zhu, X. Chen and X. Liu, Tuning upconversion through energy migration in core–shell nanoparticles, *Nat. Mater.*, 2011, **10**, 968–973.

45 N. Bogdan, F. Vetrone, G. A. Ozin and J. A. Capobianco, Synthesis of ligand-free colloidally stable water dispersible brightly luminescent lanthanide-doped upconverting nanoparticles, *Nano Lett.*, 2011, **11**(2), 835–840.

46 H. Schafer, P. Ptacek, H. Eickmeier and M. Haase, Synthesis of Hexagonal Yb3R,Er3R-Doped NaYF4 Nanocrystals at Low Temperature, *Adv. Funct. Mater.*, 2009, **19**, 3091–3097.

47 J. C. Boyer, L. A. Cuccia and J. A. Capobianco, Synthesis of Colloidal Upconverting NaYF4: Er3/Yb3 and Tm3/Yb3 Monodisperse Nanocrystals, *Nano Lett.*, 2007, **7**, 847–852.

48 J. C. Boyer, F. Vetrone, L. A. Cuccia and J. A. Capobianco, Synthesis of Colloidal Upconverting NaYF4 Nanocrystals Doped with Er3,Yb3 and Tm3 ,Yb3 *via* Thermal Decomposition of Lanthanide Trifluoroacetate Precursors, *J. Am. Chem. Soc.*, 2006, **128**, 7444–7445.

49 R. H. Page, K. I. Schaffers, P. A. Waide, J. B. Tassano, S. A. Payne, W. F. Krupke and W. K. J. Bischel, Upconversion-pumped luminescence efficiency of rare-earth-doped hosts sensitized with trivalent ytterbium, *J. Opt. Soc. Am. B*, 1998, **15**(3), 996–1008.

50 Q. Liu, W. Feng, T. Yang, T. Yi and F. Li, Upconversion luminescence imaging of cells and small animals, *Nat. Protoc.*, 2013, **8**, 2033–2044.

51 R. Krishnana and J. Thirumalai, Up/down conversion luminescence properties of (Na0.5Gd0.5)MoO4:Ln3+ (Ln = Eu, Tb, Dy, Yb/Er, Yb/Tm, and Yb/Ho) microstructures: synthesis, morphology, structural and magnetic investigation, *New J. Chem.*, 2014, **38**, 3480–3491.

52 X. Chen, J. Vanacken, J. Han, Z. Zhong, L. Li, Y. Han, Y. Liu and V. V. Moshchalkov, Intense infrared upconversion luminescence of NaGdF4:Yb/Tm with controlled intensity, *J. Appl. Phys.*, 2017, **121**, 163103.

53 A. Yin, Y. Zhang, L. Sun and C. Yan, Colloidal synthesis and blue based multicolor upconversion emissions of size and composition controlled monodisperse hexagonal NaYF4 : Yb,Tm nanocrystals, *Nanoscale*, 2010, **2**, 953–959.

54 I. Kamińska, K. Fronc, B. Sikora, M. Mouawad, A. Siemiarczuk, M. Szewczyk, K. Sobczak, *et al.*, Upconverting/magnetic: Gd2O3:(Er3+,Yb3+,Zn2+) nanoparticles for biological applications: effect of Zn2+ doping, *RSC Adv.*, 2015, **5**, 78361–78373.

55 G. Seisenberger, M. U. Ried, T. Endress, H. Buning, M. Hallek and C. Brauchle, Real-time single-molecule imaging of the infection pathway of an adeno-associated virus, *Science*, 2001, **294**(5548), 1929–1932.

56 W. M. Leevy, S. T. Gammon, H. Jiang, J. R. Johnson, D. J. Maxwell, E. N. Jackson, *et al.*, Optical imaging of bacterial infection in living mice using a fluorescent nearinfrared molecular probe, *J. Am. Chem. Soc.*, 2006, **128**, 16476–16477.

57 L. Q. Xiong, M. X. Yu, M. J. Cheng, M. Zhang, X. Y. Zhang, C. J. Xu, *et al.*, A photostable fluorescent probe for targeted imaging of tumour cells possessing integrin avb3, *Mol. BioSyst.*, 2009, **5**, 241–243.

58 M. Zhang, M. X. Yu, F. Y. Li, M. W. Zhu, M. Y. Li, Y. H. Gao, *et al.*, A highly selective fluorescence turn-on sensor for cysteine/homocysteine and its application in bioimaging, *J. Am. Chem. Soc.*, 2007, **129**(34), 10322–10323.

59 M. X. Yu, Q. Zhao, L. X. Shi, F. Y. Li, Z. G. Zhou, H. Yang, *et al.*, Cationic iridium(III) complexes for phosphorescence staining in the cytoplasm of living cells, *Chem. Commun.*, 2008, 2115–2117.

60 M. Bruchez Jr, M. Moronne, P. Gin, S. Weiss and A. P. Alivisatos, Semiconductor nanocrystals as fluorescent biological labels, *Science*, 1998, **281**, 2013–2016.

61 W. C. W. Chan and S. Nie, Quantum dot bioconjugates for ultrasensitive nonisotopic detection, *Science*, 1998, **281**(5385), 2016–2018.

62 B. Dubertret, P. Skourides, D. J. Norris, V. Noireaux, A. H. Brivanlou and A. Libchaber, In vivo imaging of quantum dots encapsulated in phospholipid micelles, *Science*, 2002, **298**, 1759–1762.

63 A. M. Smith, H. W. Duan, A. M. Mohs and S. M. Nie, Bioconjugated quantum dots for in vivo molecular and

cellular imaging, *Adv. Drug Delivery Rev.*, 2008, **60**, 1226–1240.

64 W. B. Cai, D. W. Shin, K. Chen, O. Gheysens, Q. Z. Cao, S. X. Wang, *et al.*, Peptide-labeled near-infrared quantum dots for imaging tumor vasculature in living subjects, *Nano Lett.*, 2006, **6**, 669–676.

65 L.-Q. Xiong, Z.-G. Chen, M.-X. Yu, F.-Y. Li, C. Liu and C.-H. Huang, Synthesis, characterization, and in vivo targeted imaging of amine-functionalized rare-earth up-converting nanophosphors, *Biomaterials*, 2009, **30**, 5592–5600.

66 D. K. Chatterjee, A. J. Rufaihah and Y. Zhang, Upconversion fluorescence imaging of cells and small animals using lanthanide doped nanocrystals, *Biomaterials*, 2008, **29**, 937–943.